Atmos. Meas. Tech. Discuss., 6, 2533–2581, 2013
www.atmos-meas-tech-discuss.net/6/2533/2013/
doi:10.5194/amtd-6-2533-2013

Atmospheric Measurement Techniques
Open Access
Discussions

Improved information about the vertical location and extent of cloud layers from POLDER3 measurements in the oxygen A band

M. Desmons, N. Ferlay, F. Parol, L. Mcharek, and C. Vanbauce

Laboratoire d'Optique Atmosphérique, UMR8518, CNRS – UFR de Physique, Université Lille 1, Villeneuve d'Ascq, France

Received: 1 February 2013 – Accepted: 28 February 2013 – Published: 12 March 2013

Correspondence to: M. Desmons (marine.desmons@ed.univ-lille1.fr)

Published by Copernicus Publications on behalf of the European Geosciences Union.

Abstract

This paper describes new advances in the exploitation of oxygen A band measurements from POLDER3 sensor aboard PARASOL, satellite platform within the A-Train. These developments result from a better account of the dependence of POLDER oxygen parameters to cloud optical thickness τ and to the scene's geometrical conditions, but also and more importantly from the finer understanding of the sensitivity of these parameters to cloud vertical extent. This sensitivity is made possible thanks to the multidirectional character of POLDER measurements. In the case of monolayer clouds that represent most of cloudy conditions, new oxygen parameters are obtained and calibrated from POLDER3 data colocalized with the measurements of the two active sensors of the A-Train, CALIOP/CALIPSO and CPR/CloudSat. From a parameterization that is (μ_s, τ) dependent, with μ_s the cosine of the solar zenith angle, a cloud top oxygen pressure (CTOP) and a cloud middle oxygen pressure (CMOP) are obtained which are estimates of actual cloud top and middle pressures. The performance of CTOP and CMOP are presented for the most numerous ISCCP cases in 2008. The coefficient of the correlation between CMOP and the actual cloud middle pressure is 0.81 for cirrostratus, 0.79 for stratocumulus, 0.75 for deep convective clouds. The coefficient of the correlation between CTOP and the actual cloud top pressure is 0.75, 0.73, and 0.79 for the same cloud types respectively. The score obtained by CTOP, defined as the confidence in the retrieval for a particular range of infered value and for a given error, is higher than the one of MODIS CTP. For liquid and ice clouds, the score reaches 50 and 70 % respectively for bin value of CTP superior in numbers and accepted errors of 30 and 50 hPa. From the difference between CTOP and CMOP, a first estimate of the cloud vertical extent H is possible. Then, the correlation between the angular standard deviation of POLDER oxygen pressure $\sigma_{P_{O_2}}$ and the cloud vertical extent is described in detail in the case of liquid clouds. The correlation is shown to be spatially and temporally robust, excepted for clouds above land during winter months. The study of the correlation's dependence to cloud optical thickness and to the scene's

AMTD
6, 2533–2581, 2013

geometrical conditions leads to parameterizations which provide a second way for retrieving H for this type of clouds. For liquid water clouds above ocean in 2008, the mean difference between the actual cloud vertical extent and the one retrieved from $\sigma_{P_{O_2}}$ (from the pressure difference) is 5 m (−12 m). The standard deviation of the mean difference is close to 1000 m for the two methods. The score of 50 % confidence for the retrieval of H corresponds to an error of 20 and 40 % for ice and liquid clouds respectively over ocean. These promising results need to be validated outside of the CALIPSO/CloudSat track.

1 Introduction

Cloud amount and the vertical distribution of cloud properties are key parameters of the climate system through their major influence on the incoming solar radiation and the outgoing thermal radiation. Heating and cooling rates within the atmosphere, fundamental driver in the climate system (Stephens, 1978; Li and Min, 2010), cannot be well estimated without a good description of the vertical cloudiness structure. Thus, among all the microphysical and macrophysical cloud properties, the cloud top pressure (CTP) and the layer geometrical thickness (H) represent very desired parameters to be retrieved. For climate studies those parameters must be provided on a global scale and satellites are the most appropriate tool. Active sensors as lidar (Winker and Trepte, 1998; Winker et al., 2007) or radar (Mace et al., 2009) have the inherent ability to provide fairly accurately the base and cloud top altitudes of cloud layers, but they suffer from poor spatial coverage. It would be very interesting and valuable to get the same information from space instruments having a large field of view like most passive instruments.

Different methods using passive measurements have been developed to infer the cloud top level from space. The most common one is the measurement of the brightness temperature at 11 µm to obtain cloud top temperature (Rossow and Schiffer, 1999). The cloud top temperature is then converted to cloud top height (CTH) or cloud top pressure via a vertical atmospheric profile. This method is well adapted to high opaque clouds but is known to be inappropriate in case of temperature inversions. For example the MODerate Resolution Imaging Spectroradiometer (MODIS) algorithm will place the cloud above the inversion that can lead to a cloud top mislocation of about 200 hPa (Menzel et al., 2008). Another method used to retrieve CTP is the so-called CO_2-slicing technique (Wielicki and Coakley, 1981) which uses radiances measured within the 15 µm CO_2 absorption region. Because of the lack of sensitivity in the lower layers of the atmosphere, MODIS uses this method only for clouds whose tops are higher than 3 km. For lower clouds MODIS algorithm reverts to the 11 µm brightness temperature method. In all cases MODIS CTP algorithm uses sounding profiles from global forecast. Cloud top level can also be obtained from high-spectral infrared sounder instruments like the Atmospheric Infrared Sounder (AIRS) (Weisz et al., 2007). One advantage of AIRS method is to simultaneously retrieve CTP and the sounding profiles. One can also mention methods that use stereo observations (Seiz et al., 2007; Wu et al., 2009) or the polarimetry of reflected sunlight (Goloub et al., 1994; Knibbe et al., 2000).

An alternative method to infer cloud top pressure is the exploitation of the absorption of solar radiation by the atmospheric oxygen molecules. Oxygen is well mixed in the atmosphere, and the depth of O_2 absorption can be related to a certain path length across the atmosphere. Above a bright surface as cloud acts in first approximation, O_2 absorption that suffers solar radiation backscattered toward a spaceborne sensor, is mainly related to the cloud vertical location and to the solar and viewing geometries. Hence the cloud top pressure can be inferred. Such methods using reflected sunlight in oxygen absorbing bands depend very weakly on the pressure/temperature vertical profiles. They do not suffer for a lack of sensitivity in case of low clouds, and are not sensitive to temperature inversions. After several theoretical studies (Wu, 1985; Fischer and Grassl, 1991; Kuze and Chance, 1994), airborne experiments (Fischer et al., 1991) and satellite missions have provided measurements in the oxygen absorption A band, a spectral domain centered at 760 nm and approximately 15 nm width (see Fig. 1).

AMTD
6, 2533–2581, 2013

Various studies have shown their capabilities to retrieve an apparent cloud pressure (Vanbauce et al., 1998; Koelemeijer et al., 2002; Fournier et al., 2006; Lindstrot et al., 2006; Preusker et al., 2007; Yang et al., 2012) using different sensors with narrow bands centered on the oxygen absorption, with different spectral characteristics and different radiative inversion model.

As it was stated very early (Yamamoto and Wark, 1961; Saiedy et al., 1965), multiple scattering within cloud layers enhances absorption of radiation by oxygen (Bennartz and Preusker, 2006) and thus affects the relevance and accuracy of the retrieved cloud pressure from A band measurements. It partly explains the gap between the apparent and the actual cloud top pressure, which has been largely recognized for the different measurement approaches described previously. It leads to a systematic overestimation of cloud top pressure (underestimation of cloud top height) (Vanbauce et al., 1998) and the apparent cloud pressure is actually close to the middle-of-cloud pressure (Vanbauce et al., 2003; Wang et al., 2008; Sneep et al., 2008; Ferlay et al., 2010). In the case of low cloud desk that evidently have a thin geometrical thickness, the bias is relatively small and the CTP can be fairly well determined, for example within 25 hPa with MERIS O_2 A band technique (Lindstrot et al., 2006).

Refering to van de Hulst (1980), Ferlay et al. (2010) simulated photon transport and radiative transfer inside cloudy atmospheres, and showed that vertical photon penetration within cloud layers depends mainly on the cloud geometrical thickness H, with an angular dependance, and so did the difference between POLDER cloud apparent pressure and actual cloud top pressure. They further analyzed that, thanks to the multiangular character of POLDER instrument, POLDER oxygen pressure product and H were potentially strongly correlated. A first intensive intercomparison of cloud layer altitudes inferred from CloudSat/CALIPSO collocated with POLDER/PARASOL measurements confirmed this correlation. Thus, the sensitivity of measurements in the oxygen A band to the unknown cloud geometrical thickness H could be exploited in order to retrieve H instead of being the most important source of errors when deriving the cloud top pressure (Preusker and Lindstrot, 2009). The present paper pursues the Ferlay

AMTD
6, 2533–2581, 2013

et al. (2010) study. Based on the same understanding of the sensitivities of POLDER oxygen pressure and on the same database, we show here how we can gain further information about unbiased cloud pressures and vertical extent.

This paper is organized as follows. In Sect. 2, we present the POLDER oxygen pressure data and algorithm and we recall the known bias and sensitivity of POLDER oxygen pressure products. In Sect. 3, we present the other A-Train data used in this study and the limitation of our dataset. In Sect. 4, we explain the principle for getting unbiased cloud top and middle pressures and the associated results. In Sect. 5, the strength and characteristics of the correlation between the angular standard deviation of POLDER oxygen pressure $\sigma_{P_{O_2}}$ and the cloud geometrical thickness H are studied. Then in Sect. 6, we compare the results obtained for the H retrieved from our two methods.

2 POLDER oxygen pressure

2.1 POLDER cloud oxygen pressure principle and algorithm

In this study, we exploit data from POLDER3 sensor on PARASOL, plateform within the Afternoon Train Atmospheric Observatory (A-Train; Stephens et al., 2002). PARASOL has been launched in 2004. PARASOL orbit has been lowered a first time in December 2009, then in November 2011, such that PARASOL does not perform as many measurements coincident with other A-Train satellites, though POLDER3 sensor still works perfectly.

POLDER cloud oxygen pressure is inferred from multidirectional (up to 14) measurements in two channels located in the oxygen A band, at around 763 and 765 nm, whose full width at half maximum (FWHM) are respectively 10 and 40 nm. Figure 1 illustrates the spectral variability of the atmospheric absorption in this domain as well as the POLDER response filters for the two channels.

AMTD
6, 2533–2581, 2013

The oxygen pressure algorithm principle is based upon the fact that O_2 absorption indicates the penetration depth of radiation within the atmosphere and therefore, the cloud top height can be estimated. The oxygen transmittance T_{O_2}, from the top of the atmosphere to a level pressure P then back to space, has been pre-calculated, assuming a perfect reflector located at pressure P. The oxygen pressure algorithm then relates the reflectance ratio measurements in the two POLDER O_2 absorption bands to T_{O_2}. Finally a cloud oxygen pressure can be determined.

Those calculations were realized with a line-by-line model (Scott, 1974) using the spectroscopic parameters from HITRAN 2004 (Rothman et al., 2005). In these simulations, the atmosphere is assumed to be a purely absorbing medium and the cloud acts as a perfect solid reflector. Thus only O_2 absorption above the cloud level is taken into account. Various geometrical conditions and standard atmospheric models have been used and a regression was performed to output a set of coefficients linking the oxygen transmittance T_{O_2} and the air-mass factor, to the reflector pressure level. As MERIS sensor, POLDER has only two large spectral bands in the oxygen A band. The oxygen transmission T_{O_2}, which cannot be measured directly, is derived from the ratio of the reflectance measured in a channel strongly influenced by oxygen absorption (narrow spectral band centered at 763 nm, FWHM of 10 nm) to the reflectance measured in a less influenced one (wide spectral band centred at 765 nm, FWHM of 40 nm). Contrary to MERIS which has two separate bands, POLDER narrow band is totally included in the wide band (see Fig. 1). Thus to infer the oxygen transmission, POLDER wide band must be first corrected for the band percentage where the oxygen lines are located (see Buriez et al., 1997 for details). In the operational algorithm, the measured reflectances at 763 and 765 nm are also corrected for gaseous absorption by water vapour and ozone.

With its CCD sensor, POLDER acquires up to 14 quasi-simultaneous observations of the same elementary pixel ($6 \times 7\,\mathrm{km}^2$) with different viewing geometries. In the Level-2 POLDER operational algorithm, the cloud pressure value affected to a super-pixel ($18 \times 21\,\mathrm{km}^2$) is determined for each viewing direction from the spatial averaging of the

AMTD
6, 2533–2581, 2013

results obtained for each elementary cloudy pixel with spherical albedo larger than 0.3 (i.e. an optical thickness τ of 2 for liquid water clouds and 3.5 for ice clouds). An additional correction is made over land surface to take into account the increase of the photon path length due to multiple scattering between the cloud and the surface (see Vanbauce et al., 2003 for details). The angular values are then averaged accounting for cloud fraction – the mean is noted P_{O_2} – and the associated angular standard deviation $\sigma_{P_{O_2}}$ is calculated. For technical reasons as well as question of cloud pressure accuracy, the averaged cloud pressure is finally rounded to the nearest 5 hPa and the angular standard deviation to the nearest 2.5 hPa.

2.2 Known bias and sensitivity to cloud vertical extent

Real clouds do not act as perfect reflecting boundaries. A consequence of it is the gap between calculated cloud oxygen pressure and actual cloud top pressure (CTP), due to the part of absorption by oxygen along photon path within cloud layers. It is particularly true for POLDER oxygen pressure estimate whose retrieval algorithm is based on that hypothesis. For example comparisons between POLDER apparent pressure and the cloud top pressure derived from METEOSAT infrared measurements showed a mean difference of 180 hPa (Vanbauce et al., 1998). Similar comparisons between POLDER apparent pressure and the International Satellite Cloud Climatology Project (ISCCP) cloud top pressure showed a bias of 140 hPa (Parol et al., 1999). More precisely, cloud oxygen pressure appears close to the pressure of the geometrical middle of cloud layer. It has been observed several time with SCIAMACHY data (Wang et al., 2008) and with POLDER data (Vanbauce et al., 2003; Sneep et al., 2008; Ferlay et al., 2010).

Actually, Ferlay et al. (2010) studied in detail the vertical photon penetration within cloud layer (noted $< Z >$), its dependence and its angular variation for different upwelling outgoing directions. For clouds optically thick enough, Monte Carlo results showed the strong dependence of $< Z >$ on the cloud geometrical thickness H, with a weaker dependence on the cloud optical thickness τ and cloud microphysical properties.

AMTD
6, 2533–2581, 2013

It confirmed the asymptotic relation $< Z >= \mu_s \mu_v H$ from van de Hulst (1980), with μ_s and μ_v the cosines of the solar and viewing zenith angles respectively.

Because the cloud oxygen pressure P_{O_2} is affected by $< Z >$, it varies accordingly: first, P_{O_2} hangs on with the upwelling outgoing directions (as illustrated in Fig. 2). Then, for clouds optically thick enough, $P_{O_2} - \text{CTP}$ depends on the cloud geometrical thickness H, and the angular standard deviation of POLDER pressure $\sigma_{P_{O_2}}$ is potentially highly correlated with H. Using a large set of POLDER data coincident with CloudSat and CALIPSO measurements, Ferlay et al. (2010) confirmed the small bias between P_{O_2} and the cloud middle pressure (CMP) for monolayer clouds, and proposed a way to reduce it. They confirmed also, thanks to the sensitivity of $\sigma_{P_{O_2}}$ to H, the possible inversion of H from $\sigma_{P_{O_2}}$ for optically thick enough clouds, ie the feasibility of retrieving cloud geometrical thickness from multidirectional measurements in the oxygen A band. Simulations with liquid and ice clouds showed the importance of the account of cloud thermodynamical phase in this inversion process.

To summarize, Ferlay et al. (2010) confirmed the closeness between POLDER oxygen pressure and cloud middle pressure. But more, their main result is the strong dependence of oxygen product on cloud geometrical thickness H. From this dependence, we can investigate further and plan to improve the significance of the retrieved cloud pressure, and invert the geometrical thickness of cloud from POLDER oxygen product. To reach these goals, we need to analyze the sensitivity of POLDER oxygen pressures and of the correlation $(\sigma_{P_{O_2}}, H)$ to cloud optical thickness τ, and to the geometrical conditions of the scene's observation. It is the purpose of the following Sects. 4, 5 and 6.

3 A-Train dataset used

In the next section we present new inferences obtained from POLDER cloud oxygen pressure Level2 parameters P_{O_2} and $\sigma_{P_{O_2}}$: new cloud pressures, and an estimate of cloud geometrical thickness. POLDER data were sampled under the CloudSat/CALIPSO track in order to get "true" cloud vertical locations from the lidar and radar echoes. The CPR radar aboard CloudSat and the CALIOP lidar aboard CALIPSO have indeed complementarity sensitivities to detect thin and thick scattering layers. This intercomparison filters daytime only CloudSat/CALIPSO data. Thus, we manipulate CALTRACK Level2 data delivered by the ICARE thematic center (web adress: http://www.icare.univ.lille1.fr/) through the MULTI_SENSOR_CALTRACK_UNIT project. The so-called CloudSat 2B_GEOPROF_LIDAR data provide cloud base and top altitudes (LAYERBASE and LAYERTOP) at a horizontal resolution of 5 km. From them, we get cloud geometrical extent H, as well as cloud base, top and middle pressures (noted CBP, CTP and CMP). We realize the altitude to pressure conversion thanks to a local altitude-pressure conversion index. This index has been added as a SDS to the CALTRACK_ L2_2B_ GEOPROF_LIDAR files. It originates, for each pixel of a granule, from the set of a 345 long vector of pressures that corresponds to 345 altitudes. These pressures are GEOS-5 DAS gridded outputs (Rienecker, 2008) produced by the NASA Global Modeling and Assimilation Office (GMAO). GMAO data consist in thermodynamic variables obtained from meteorological re-analyses (Bloom et al., 2005) and are available with CALIPSO CAL_ LID_L2_ 05kmCPro files. From this index and the pressure vector, a pressure can be obtain from any given altitude (here we get CTP and CBP from LAYERTOP and LAYERBASE and CMP from the combination of LAYERBASE and LAYERTOP). All the data used in this study are listed in Table 1. MODIS data are used as a reference or to filter further data.

To exploit and analyze the expected information contained in POLDER A band measurements, we restricted our study to cloud layers the closest to homogeneous plane-parallel desk, optically thick enough and whose thermodynamical phase is similar when identified by POLDER or MODIS. We realized the first condition through a data filtering: clouds are monolayered ($n = 1$), with no clear air fraction (POLDER fractional cloud cover "cc" – at the resolution of $18 \times 21\ \mathrm{km}^2$ – is larger than 0.95). However, it is obvious that ice clouds that have a large vertical extent of several kilometers are necessary

Discussion Paper | Discussion Paper | Discussion Paper | Discussion Paper |
AMTD
6, 2533–2581, 2013

often more distant to the model of the homogeneous plane-parallel slab. For the second condition we retained clouds with $\tau \geq 5$. Indeed, Ferlay et al. (2010) have shown that $\sigma_{P_{O_2}}$ and the cloud vertical extent H were correlated for liquid water clouds with $\tau \geq 5$ and for ice clouds with $\tau \geq 10$. Thanks to a deeper sensitivity study, it appears that this correlation stays high for $\tau \geq 5$ whatever the thermodynamic phase.

In the rest of the paper, cloud's climatology and statistics shown will only concern monolayered cloud covers filtered as indicated above. To figure out what this filtering represents, here are some numbers: in 2008, monolayer clouds are 64 %, clouds for which the POLDER fractional cloud cover is higher than 0.95 represent 87 %, and clouds with optical thickness larger than 5 are 73 %, of the whole clouds overcast. So that monolayered, very much covered, and optically thick enough clouds correspond to 47 % of all clouds detected in 2008 under the CloudSat/CALIPSO track. Figure 3 shows the occurence of monolayered and multilayered clouds as a function of the latitude by 5° bins. The occurrence of multiple layers is a strong function of latitude: monolayered clouds are in the majority over almost the entire planet except over the equator and the subtropical areas (for latitudes between −20 and +20°) where the tendency is the opposite. Among monolayered clouds, 53% are liquid ones while about 27 % are ice clouds. If we look at their geographical distribution, we notice that liquid clouds are predominant except for latitudes between −5 and +15°.

To understand which cloud population is concerned in this study, we plot in Fig. 4 CALIOP/CloudSat CTP-H diagrams for ice (panel a) and liquid (panel b) clouds distinguishing ocean (left) from land (right). The altitude of ice clouds are not surprinsingly quite high – the mean CTP is 250 hPa over land and 240 hPa over ocean – and geometrically thick whatever the surface. The main difference between land and ocean is that there are much more thinner cirriform clouds over land than over ocean (2000–7000 m), which is consistent with the climatologies established by Stubenrauch et al. (2006) and Warren et al. (2012). Concerning liquid clouds, Fig. 4 shows that there are more clouds at higher altitudes and vertically more extended over land than over ocean. This observation is coherent with Stubenrauch et al. (2006) and Wang et al.

AMTD
6, 2533–2581, 2013

(2000), and may be explained by the height of the land surface which is about 500 m from the mean sea level and the highest occurence of low-level cloudiness over ocean.

4 New POLDER oxygen pressures

Thanks to their analyze of the vertical penetration of photons within cloud layer as well as the distance between POLDER oxygen pressures and actual cloud top pressure, Ferlay et al. (2010) have allowed to get a better significance of the inferred oxygen pressures. Here, we pursue this effort by accounting for the double dependence of cloud inferred pressures to cloud optical thickness and solar zenith angle (or its cosine μ_s). We show that we can obtain unbiased estimates of cloud middle and top pressures.

To evaluate the relevance of these pressures, we make use of the International Satellite Cloud Climatology Project (ISCCP) definitions (Rossow and Schiffer, 1999) to distinguish high clouds (CTP < 440 hPa), midlevel clouds (440 hPa < CTP < 680 hPa) and low clouds (CTP > 680 hPa). High clouds can be further separated into cirrus ($\tau < 3.6$), cirrostratus ($3.6 < \tau < 23$) and deep convective clouds ($\tau > 23$). Midlevel clouds are separated into altocumulus ($\tau < 3.6$), altostratus ($3.6 < \tau < 23$) and nimbostratus ($\tau > 23$). At last, among low clouds, we find cumulus ($\tau < 3.6$), stratocumulus ($3.6 < \tau < 23$) and stratus ($\tau > 23$). In this study, we work on clouds for which $\tau > 5$, consequently cirrus, altocumulus and cumulus are not represented here. Low and middle clouds are also classified according to their thermodynamical phase although all high clouds are ice.

4.1 Unbiased estimate of cloud middle pressure: principle and results

Ferlay et al. (2010) studied the difference between P_{O_2} and the pressure of the cloud's midlevel (CMP). Here we keep making the distinction between liquid and ice clouds, and we go further by accounting for the dependence, not only on cloud optical thickness, but also on the solar zenith angle. Figure 5 shows the difference on average between POLDER oxygen pressures and actual cloud middle pressure (CMP) obtained from CloudSat/CALIPSO, for liquid clouds (panel a) and ice clouds (panel b).

It shows that the higher the sun, the higher is the POLDER oxygen pressure P_{O_2}. This is because the pathlength of photons within cloud layers is enhanced when the sun is high, or equivalently that they penetrate more within the clouds. Figure 5 shows also the sensitivity of the pressure's difference to cloud optical thickness τ. This sensitivity is low for liquid clouds while high for ice clouds. For liquid clouds on average, $P_{O_2} - \mathrm{CMP}$ does not depend much on cloud optical thickness for $\tau \geq 20$. For ice clouds, the absolute value of $P_{O_2} - \mathrm{CMP}$ is smaller than 50 hPa when $\tau \geq 40$, and much larger for lower values of τ.

The principle for obtaining an estimate of CMP from POLDER oxygen pressures P_{O_2} is the following: if $P_{O_2} - \mathrm{CMP} = f(\tau, \mu_s)$, then $P_{O_2} - f(\tau, \mu_s)$ should provide a good estimate of CMP. Hereafter, we note CMOP the quantity $P_{O_2} - f(\tau, \mu_s)$, that stands for cloud middle oxygen pressure. We obtained CMOP after a fit of the functions shown in Fig. 5 with 3rd-order polynomials.

Figure 6 shows the comparison between CMOP and CloudSat/CALIPSO CMP for the four most numerous ISCCP cases in 2008. CMOP was obtained from a parameterization based on 2008 data. Correlations for the years 2007, and 2009–2010, are close to the ones shown here. Also not shown is the comparison for stratus liquid clouds, for which the correlation is around 0.747. The best results are obtained for ice clouds with high correlation, small bias and regression's slope close to unity. Comparisons for liquid low level clouds show a larger bias, that might be due to the effect of Rayleigh scattering above the cloud layers. The result is worse for mid-level clouds with a correlation of 0.54.

4.2 Unbiased estimate of cloud top pressure: principle and results

Because the difference between P_{O_2} and the actual cloud top pressure CTP is mainly a function of the cloud geometrical thickness H, and because H is potentially strongly correlated with $\sigma_{P_{O_2}}$ (Ferlay et al., 2010) as will be shown in detail in Sect. 5, we though about correcting P_{O_2} from its bias to CTP by exploiting the relation between P_{O_2} – CTP as a function of $\sigma_{P_{O_2}}$. If indeed P_{O_2} – CTP $= f(\sigma_{P_{O_2}})$, then $P_{O_2} - f(\sigma_{P_{O_2}})$ should be an unbiased estimate of CTP: we would unbiase P_{O_2} with a parameterization which depends on an "observable", $\sigma_{P_{O_2}}$. Hereafter, we note CTOP the quantity $P_{O_2} - f(\sigma_{P_{O_2}})$, that stands for cloud top oxygen pressure. Figure 7 shows an exemple of functions $f(\sigma_{P_{O_2}})$ for the case of liquid clouds over ocean in 2008, and for solar zenith angles such that $0.7 \leq \mu_s \leq 0.8$.

Not surprizingly, the difference P_{O_2} – CTP increases with $\sigma_{P_{O_2}}$: as clouds move away from the asymptotic model of a perfect reflector (for which $\sigma_{P_{O_2}}$ would equal zero), P_{O_2} becomes larger than CTP. We obtained CTOP after a 3rd-order polynomial fit of the functions $f(\sigma_{P_{O_2}})$ like the ones shown in Fig. 7.

To evaluate the relevance of the pressure CTOP, we classify again liquid and ice clouds according to the ISCCP cloud types. The right panels of Fig. 8 show the comparison between CTOP and CloudSat/CALIPSO CTP for the four most numerous ISCCP cases in 2008. CTOP was obtained from a parameterization based on 2008 data. The center panels show for comparison the relation between POLDER cloud pressure P_{O_2} and CTP. The left panels show for reference the relation between MODIS CTP and CTP.

Correlations obtained for the years 2007, and 2009–2010, are again close to the ones shown here. Figure 8 shows a decrease of the bias – from POLDER pressures P_{O_2} to CTOP – compared with CTP, that can be spectacular for clouds with a high vertical extent (cases a, b and c). In the case of liquid altostratus clouds (case c), the feature of the 2-D plot for CTOP and MODIS CTP (right and left panels respectively) is quite different. This is due to the fact that numerous clouds with actual CTP < 580 hPa come with biased new oxygen inference with CTOP > 600 hPa. For low level liquid clouds (case d), the new POLDER pressure CTOP is again statistically closer to CTP than P_{O_2}. A slight bias still exists however, which might be due again to the effect of Rayleigh scattering above the cloud layers. For this last case, CTOP seems more

AMTD
6, 2533–2581, 2013

relevant than Collection 5 MODIS CTP whose known issue (Holz et al., 2008) is evident on the left panel of Fig. 8, case d. To go further in the evaluation of the new POLDER pressure CTOP, we computed the score obtained by CTOP, defined as the occurence of CTP estimates less than a given value away from the actual value of cloud top pressure given by CALIPSO/CloudSat. The score corresponds thus to the confidence in the cloud top pressure retrieval for a given accuracy. Left panels in Fig. 9 show such scores over ocean surfaces for different classes of CTP. For liquid water clouds (case a), scores on the left correspond to a distance of 30 hPa. For ice clouds (case b), the distance considered is 50 hPa. For liquid clouds, the score obtained by CTOP is slightly higher than the one of MODIS CTP for pressures smaller than 600 hPa, but for most cases, the score for CTOP is much better, reaching 50 % for pressures close to 800 hPa (majority of cases), and even 65 % for clouds with pressure around 950 hPa, against 35 % maximum for MODIS CTP. The global scores – on the right – are thus better for CTOP than for MODIS CTP, regardless of the error given (for example 45 % against 25 % for a 30 hPa difference, 65 % against 40 % for 50 hPa). It confirms again the issue with the MODIS pressure inference of low level clouds CTP. For ice clouds and an error of 50 hPa (case b, left panel), scores obtained by MODIS CTP are significantly higher than the one of CTOP when pressures are smaller than 200 hPa. Otherwise, scores of MODIS CTP and CTOP are close, with scores of CTOP slightly better, especially at low altitudes. The global scores for ice clouds – case b on the right – are slightly better for CTOP than for MODIS CTP, especially for errors less than 80 hPa (for example 48 % against 38 % for a 40 hPa difference).

Above land, correlations – not shown here – between CTOP and CTP, CMOP and CMP, do not change very much. The correlations tend to be slightly lower above land for most cases. It can be understood because of the surface effect, even if this effect is accounted for in the POLDER oxygen pressure algorithm. However, correlations above land are higher for low level liquid clouds (between 0.04 and 0.07 higher). These higher correlations can be explained by the fact that the ranges of CMP and CTP values are

AMTD
6, 2533–2581, 2013

larger above land compared with ocean. But the number of cases above land is ten times smaller compared with ocean, that limits the comparison.

To summarize, we obtained new pressures – CMOP and CTOP – which are statistically not so far from unbiased estimates of actual cloud middle and top pressures of monolayer liquid as well as ice cloud covers. From the difference between these two new pressures, we shall obtain a first estimate of the cloud vertical extent H. In Sect. 6, we evaluate the quality of this estimate of H. We shall see that the biases of CMOP and CTOP will compensate while calculating the estimate of H from their difference between CMOP and CTOP for liquid clouds over ocean, but less over land.

5 Correlation between $\sigma_{P_{O_2}}$ and the cloud vertical extent

As recalled in Sect. 2.2, the angular standard deviation $\sigma_{P_{O_2}}$ of POLDER oxygen pressure is sensitive to the cloud geometrical thickness H, and consequently there is a potential to retrieve H from $\sigma_{P_{O_2}}$ for optically thick enough clouds. Ferlay et al. (2010) showed this potential for liquid water clouds from simulations and measurements. In this section, we go further and show the strength of the correlation between $\sigma_{P_{O_2}}$ and H with a spatial and temporal study of the relation H–$\sigma_{P_{O_2}}$. We also study the complex sensitivity of the relation between H and $\sigma_{P_{O_2}}$ to the cloud's optical thickness and to the scene's geometrical conditions. The detailed study of this sensitivity will lead to improved retrieval of H from $\sigma_{P_{O_2}}$. While the correlation exists also theoretically in the case of ice clouds, we show here results for liquid clouds only as the correlation observed between H and $\sigma_{P_{O_2}}$ is not straightforward for ice clouds. This is certainly due to their more complex microphysics, and their enhanced heterogeneities along thousands of vertical meters.

AMTD
6, 2533–2581, 2013

5.1 Spatial variability of the correlation

In a first step, we study the spatial variability of the correlation between $\sigma_{P_{O_2}}$ and H at the global scale. To realize that, (i) data are sorted in bins of 10° of latitude, 20° of longitude and 1 km width of geometrical thickness. The spatial grid (10 × 20°) and the size of geometrical thickness class have been determined in order to optimize the correlation; (ii) for each area and for each geometrical thickness class, the average and the standard deviation of $\sigma_{P_{O_2}}$ are calculated; (iii) these two quantities are used in the *pearsn* routine (Press et al., 1992) that provides for each area the correlation coefficient r and the slope S of the linear regression between $\sigma_{P_{O_2}}$ and the center of each geometrical thickness bin.

Figure 10 represents the spatial distribution of the correlation coefficient r between $\sigma_{P_{O_2}}$ and H for monolayered liquid water clouds in 2008. It shows that r is high for most areas in both hemispheres: r is higher than 0.8 for 162 over 283 cases. The correlation coefficient can be however very low in several areas, in particular over land, over the Asian continent, Australia and for very high latitudes. We also see an anti-correlation (r close to -1) over the North-East of Africa. To summarize, for liquid clouds, the correlation between $\sigma_{P_{O_2}}$ and H is high for most meshes over oceans, and for half of the cases over land. This figure underlines the importance of distinguishing the oceans from the continents for following studies. Not shown here, an other map of correlation coefficient for monolayered ice clouds has been realized, however the correlation is globally low in this case: r is higher than 0.8 only for 46 over 277 regions for which it was defined (in some areas, as for high latitudes, there were not enough clouds corresponding to our criterias to calculate the correlation coefficient). This is the reason why the present section focuses only on liquid water clouds.

AMTD
6, 2533–2581, 2013

5.2 Temporal variability of the correlation

In a second step, we study the temporal variability of the relation between $\sigma_{P_{O_2}}$ and H. For three years of data (2007 to 2009), we calculated the monthly mean correlation coefficient r with the same procedure as previously explained, and the slope S of the linear regression between $\sigma_{P_{O_2}}$ and H when $r > 0.8$. Figure 11 shows the temporal evolution of r and S for monolayered liquid clouds over 2007–2009 while distinguishing land surfaces from oceans in each hemisphere. Panel (a) demonstrates that the correlation is temporally robust over ocean all over the years. It also shows that the correlation stays high over land surfaces except in the winter months of each hemisphere. This decreasing of the correlation can be explained by the effect of brighter land surfaces not well accounted for by the POLDER algorithm, and smaller number of liquid cloud cases over land in winter. It can explain the weak correlation that we observe over land in Fig. 10, particularly over Asian continent at high latitudes. Panel (b) of Fig. 11 shows the temporal variability of the slope of the linear regression between $\sigma_{P_{O_2}}$ and H. Slopes are on average around 3 hPa km^{-1}, with a weak temporal variability over ocean and a higher one over land. This higher temporal variability can be explained by the stronger inter-annual variability of clouds over land than over ocean (Stubenrauch et al., 2006). These temporal variations in the slope, for most cases not far from the value 3.2 hPa km^{-1} found by Ferlay et al. (2010), suggest that a retrieval of H from $\sigma_{P_{O_2}}$ based on a unique inversion obtained at global scale should lead to better results over ocean than land, and should account for the surface type. It suggests also the robustness and the universality of the statistical relation between $\sigma_{P_{O_2}}$ and H. However, to go further, it is important to account for the dependence of this relation to cloud and other scene parameters.

AMTD
6, 2533–2581, 2013

5.3 Angular and cloud optical thickness dependences

The two previous subsections showed the spatial and temporal characteristics of the correlation between the cloud geometrical extent and the angular standard deviation of the oxygen pressure. It explains why a previous study by Ferlay et al. (2010) leads to an acceptable technique of inversion for the ensemble mean of H. However, previous simulations and results of Sect. 4 have shown the influence of cloud optical thickness and solar zenith angle on cloud oxygen pressure. These parameters affect also the relation between $\sigma_{P_{O_2}}$ and H, and this dependence has to be accounted for to reach the goal of an improved retrieval of H from oxygen A band measurements.

Figure 12 shows the amplitude of this dependence and the complexity of the relation between $\sigma_{P_{O_2}}$ and H for monolayered liquid water clouds in 2008 over ocean: for a given value of $\sigma_{P_{O_2}}$, several H are observed on average for various classes of cosine of solar zenith angle μ_s and cloud optical thickness τ. For example, an optically thin cloud with small vertical extent will lead to the same $\sigma_{P_{O_2}}$ as an optically thick cloud with large vertical extent.

In order to retrieve H from $\sigma_{P_{O_2}}$, we built parameterizations taking into account the cloud optical thickness τ and the cosine of the solar zenith angle μ_s. We sorted cloudy pixels into 10 classes over ocean (as illustrated in Fig. 12) and 6 ones over continents. Fits of fifth order were obtained and they provide the set of coefficients linking $\sigma_{P_{O_2}}$ to H for each $(\mu_s;\tau)$ classes. Exploitation of the ($\sigma_{P_{O_2}}$–H) fits and value of the inferred vertical geometrical thickness are discussed in Sect. 6.

6 Information about cloud vertical extent: synthesis

We have described two ways to retrieve cloud vertical extent from POLDER3 data. The first one takes advantage of unbiased estimates of cloud pressures, illustrated in Sect. 4. Indeed, cloud top and middle oxygen pressures (CTOP and CMOP) can

Discussion Paper | Discussion Paper | Discussion Paper | Discussion Paper |
AMTD
6, 2533–2581, 2013
Improved information about clouds from POLDER3
M. Desmons et al.

be converted to altitudes and their difference provides in principle half of the cloud vertical extent. This method is applied here for both liquid and ice clouds. The second method takes advantage of the correlation between the angular standard deviation of the oxygen pressure and the cloud geometrical thickness. As described in Sect. 5.3, a $(\mu_s;\tau)$ parameterization makes possible the retrieval of H from $\sigma_{P_{O_2}}$. At the present time, this second method is only applied to liquid water clouds.

In the following, we will note the vertical extent retrieved from the difference of pressures $H_{\Delta P}$ and the vertical extent retrieved from $\sigma_{P_{O_2}}$ H_σ. For liquid water cloudy pixels H_{mean} stands for the average of $H_{\Delta P}$ and H_σ.

Figure 13 shows the histograms of the difference between CloudSat/CALIPSO H and the retrieved one for clouds over ocean in 2008.

For liquid water clouds, the histogram of $\Delta H_\sigma = H_\sigma - H$ is almost centered on zero: $\overline{\Delta H_\sigma} = 5\,\text{m}$ with a standard deviation SD = 964 m and a median MD = 180 m. The histogram of $\Delta H_{\Delta P} = H_{\Delta P} - H$ is slightly off-centered: $\overline{\Delta H_{\Delta P}} = -12\,\text{m}$, SD = 1193 m, but the median is lower MD = −21 m. For ΔH_{mean}, $\overline{\Delta H_{\text{mean}}} = -17\,\text{m}$, SD = 983 m and MD = 73 m, which shows that the vertical extents retrieved by the two methods are consistent pixel by pixel. Results are synthetized in Table 2.

For liquid clouds over land, histograms are not shown here but characteristics of the estimates are also given in Table 2. The averages of the differences are quite different: $\overline{\Delta H_\sigma} = 23\,\text{m}$ and $\overline{\Delta H_{\Delta P}} = -272\,\text{m}$. Defining an average estimate H_{mean} appears in that case not very relevant as $\overline{\Delta H_{\text{mean}}}$ equals −138 m, much away from zero than ΔH_σ. For ice clouds over ocean, $\overline{\Delta H_{\Delta P}} = 1580\,\text{m}$ with SD = 5803 m and MD = −26 m. These values are very high compared to the liquid water cloud ones, but ice clouds have generally a much larger vertical extent than liquid water clouds and consequently the difference are relatively less important in front of the ice clouds vertical extents. For ice clouds over land, histogram of $\Delta H_{\Delta P}$ is sharper than over ocean. It is partly due to the population of ice clouds over land that contains more clouds with vertical extent below 7000 m and less clouds with H above 10 000 m (see Fig. 4).

AMTD
6, 2533–2581, 2013

Figure 13 showed the annual difference ΔH between the retrieved cloud vertical extent and the actual CloudSat/CALIOP one over the year 2008. In order to analyze the robustness of our retrieval, we studied the temporal evolution of the monthly mean of ΔH. Figure 14 shows the mean differences of ΔH_σ (solid lines) and $\Delta H_{\Delta P}$ (dashed lines) month by month from 2007 to 2009 above land (red curves) and ocean (blue curves).

For liquid water clouds (panel a), the monthly mean $\overline{\Delta H_\sigma}$ is low over the three years over ocean and land with values between −100 m and +100 m. Averages are −7 m and −9 m over ocean and land respectively and the standard deviation is close to 1000 m whatever the surface. During the same period, the monthly mean $\overline{\Delta H_{\Delta P}}$ is low over ocean with values between −100 m and +100 m but more away from zero over land where the values range from −200 m and −400 m. The averages are −20 m over ocean and −294 m over land and the standard deviation is higher (1500 m) over land than over ocean (1100 m). These observations are consistant with Fig. 13. The low performance of the pressures method to retrieve H for liquid clouds over land can be explained by the bias in inference of CMP and CTP for low level clouds mentioned in Sect. 4.2; this type of clouds representing the majority of liquid clouds, their characteristics influence the statistic. For ice clouds (panel b of Fig. 14), differences observed in 2008 are also observed month by month: they are higher compared with liquid clouds, $\overline{\Delta H_{\Delta P}} = 1375$ m above ocean, and $\overline{\Delta H_{\Delta P}} = 936$ m above land. The standard deviation is almost the same during the three years and whatever the surface, it is close to 5000 m. However, contrary to what we observe for liquid clouds, there is no important difference in the performance of $H_{\Delta P}$ over ocean and land. This could be explain by the fact that surface effects are smaller in the case of ice clouds (clouds are on average thicker and at higher altitudes). There is a clear trend in the difference for ice clouds with higher values in 2007 downto lower values in 2009. This trend is questionable. It might be due to the fact that the parameterization for retrieving H has been learned in 2008, and applied over 2007 and 2009. Not shown here, we observe also that, while

AMTD
6, 2533–2581, 2013

the CloudSat/CALIPSO monthly mean of H for ice clouds are stable over three years, the ones we retrieve decrease slightly.

This first analysis of the biases of cloud vertical extent estimates leads to the choice of H_σ as estimate of H for liquid water clouds, while for ice clouds, H is estimated by $H_{\Delta P}$.

A further analysis of the POLDER estimates of the liquid water cloud vertical extents shows an overestimation of H for some of the thinnest clouds, and an underestimation for some of the thickest. These tendencies are not surprizing considering the physical principle of the retrieval. For ice clouds, the vertical extent of the thickest clouds (more than 12 km) are either underestimated, or overestimated as for some of the thinnest ice clouds. These results are illustrated on Fig. 15 that shows histograms of cloud geometrical thickness for which the retrieval of H is close to the actual one (blue line), and far from it (thin dark green and black lines), the distance criteria being the standard deviation given in Table 2.

As for cloud top pressure estimates, we computed the score obtained by the estimate of H. It is defined as the occurence of H estimates less than a given percent away from the actual value of H given by CALIPSO/CloudSat. The score corresponds thus to the confidence in the cloud vertical extent's retrieval for a given accuracy. Global scores for liquid water and ice clouds are shown in Fig. 16 for different accuracies between 5 % and 100 %. Scores are higher for ice clouds. The fact that H for ice clouds are often much larger that for liquid water clouds explains mainly this difference. Scores are also lower over land. Figure 16 shows for example that scores obtained by POLDER estimates of cloud vertical extent, for a 30 % retrieval error, are around 70, 60, 40 and 30 % for respectively ice clouds over ocean, over land, liquid water clouds over ocean and land. Alternatively, Fig. 16 shows that scores equal to 50 % come with a retrieval error of 20, 26, 42 and 53 % for respectively ice clouds over ocean, over land, liquid water clouds over ocean and land.

AMTD
6, 2533–2581, 2013

Improved information about clouds from POLDER3

M. Desmons et al.

7 Conclusions

The perspective of retrieving the vertical location of cloud cover, ie both their top altitude (or pressure) and vertical extent from satellite passive measurements is challenging and very interesting for a broad range of applications in atmospheric sciences. Ferlay et al. (2010) showed the potential of POLDER oxygen A band measurements to reach this goal. Pathlength of solar reflected photons within clouds varies with the viewing zenith angle and so does consequently their absorption by oxygen. This leads to an angular variation of POLDER oxygen pressure, quantified by its angular standard deviation $\sigma_{P_{O_2}}$, which is correlated with the cloud geometrical thickness.

In the present study, we confirm the potential of POLDER measurements with a more detailed study of the complex relation between POLDER oxygen parameters, actual cloud top pressure and cloud vertical extent. This was possible thanks to the richness of the collocated and quasi-simultaneous observations from POLDER3 on PARASOL and the active sensors CPR/CloudSat and CALIOP/CALIPSO over years.

We show here the possibility of providing a cloud top oxygen pressure (CTOP) and a cloud middle oxygen pressure (CMOP) which are unbiased estimates of actual cloud top and middle pressures. These two new pressures are obtained from parameterizations that are $(\mu_s;\tau)$ dependent, with μ_s the cosine of the solar zenith angle and τ the cloud optical thickness. The performance of these retrievals are presented by classes of ISCCP clouds. For clouds with a high vertical extent (deep convective clouds, cirrostratus or altostratus), the results are very interesting as CTOP appears much closer to the actual CTP than P_{O_2}. For low level liquid clouds (CTP > 680 hPa), POLDER retrieval tend to slightly underestimate the actual cloud top and middle pressures. But the scores obtained by POLDER cloud top pressure estimates are interesting and high where cloud populations are the highest. They reach 60 % considering a retrieval error of plus or minus 30 and 50 hPa (for liquid and ice clouds respectively). Global scores are higher for ice clouds compared with liquid water clouds for a given pressure error. However, it does not simply signify that the accuracy of the inferred cloud top altitude is better for liquid water compared with ice clouds. The vertical variation of the atmospheric pressure is indeed much faster at low altitude compared with high altitude (the pressure gradient at 1000 hPa is approximately twice the one at 400 hPa). Hence, the global score obtained for liquid clouds and a given error should be compared with the one for ice clouds and an half error, for the same uncertainty on the cloud top altitude.

From the difference between CMOP and CTOP, one can provide in principle a first estimate of the cloud vertical extent H, $H_{\Delta P}$, although $H_{\Delta P}$ may suffer from the add of the retrieval biases of CMOP and CTOP. A second estimate H_σ is obtained directly from the correlation between $\sigma_{P_{O_2}}$ and H. This correlation is shown to be complex, but also spatially and temporally robust for liquid water clouds, particularly for those over ocean. The study of this correlation lead us to establish ten $(\mu_s;\tau)$ parameterizations for liquid water clouds over ocean and six over land which allow us to retrieve H from $\sigma_{P_{O_2}}$. Thus, we obtain two estimates of H, $H_{\Delta P}$ and H_σ for liquid clouds. Over ocean, we show that the two estimates are consistent at the pixel level with close performances. Over land, $H_{\Delta P}$ underestimates slightly on average the retrieval of H. For ice clouds, the vertical extent of clouds are estimated with $H_{\Delta P}$ only. For these clouds, the differences are in average much larger in absolute value compared with the liquid case, but the relative differences are lower.

The POLDER estimates of cloud vertical extent shown here are new and the results given here are, in a way, preliminary. The vertical extent of thin (respectively thick) liquid water clouds tends to be overestimated (underestimated), while the vertical extent of thick ice clouds tends to be underestimated) (see on Fig. 15). The case of ice clouds is more complex to handle, and so far, their vertical extent is not obtained from $\sigma_{P_{O_2}}$ but from CMOP and CTOP. This is certainly due to their more complex microphysics, from their enhanced diversity and heterogeneities along thousands of vertical meters. Despite the limits of our current retrieval, we obtain confidence scores for cloud top pressure and geometrical thickness estimates that are interesting and yet high for some cases. With CTOP and our estimate of H, CTP-H diagrams can be produced. Figure 17 shows such climatological diagram for ice clouds over ocean. The comparison with the

AMTD
6, 2533–2581, 2013

"true" one on the left panel of Fig. 4, case (a), shows that the main feature of the climatology is obtained.

Thus, the results presented in this study are promissing and encouraging, since getting complete information about cloud vertical location from a passive instrument and consequently at global scale is new. In the future, progress in the understanding of the relation between the cloud vertical extent and the angular variation of the POLDER oxygen pressure for the ice cloud case are expected. It is also necessary to evaluate the performance of our cloud retrievals outside the CloudSat/CALIPSO track. Lastly, in order to make our retrieval methods operational, an important point is the identification of the mono/multilayer character of cloud cover over the entire POLDER swath.

Acknowledgements. This study has been financed through grants from the french research CNRS program PNTS (Programme National de Télédétection spatiale) and CNES program TOSCA (Terre, Océan, Surfaces continentales, Atmosphère). We are grateful to the ICARE centre (http://www.icare.univ-lille1.fr/) for providing easy access to CALIPSO-collocated PARASOL, CloudSat, and MODIS data (MULTI_SENSOR data project) as well as computing resources.

The publication of this article is financed by CNRS-INSU.

AMTD

6, 2533–2581, 2013

Improved information about clouds from POLDER3

M. Desmons et al.

References

Bennartz, R. and Preusker, R.: Representation of the photon pathlength distribution in a cloudy atmosphere using finite elements, J. Quant. Spectrosc. Ra., 98, 202–219, 2006. 2537

Bloom, S. and da Silva, A., and Dee, D.: Documentation and validation of the Goddard Earth Observing System (GEOS) Data Assimilation System-Version 4, Tech. Rep. 165 pp., Series on Global Modeling and Data Assimilation, NASA Tech. Memo. NASA/TM-2005-104606, 2005. 2542

Buriez, J., Vanbauce, C., Parol, F., Goloub, P., Herman, M., Bonnel, B., Fouquart, Y., Couvert, P., and Sèze, G.: Cloud detection and derivation of cloud properties from POLDER, Int. J. Remote. Sens., 18, 2785–2813, 1997. 2539

Ferlay, N., Thieuleux, F., Cornet, C., Davis, A. B., Dubuisson, P., Ducos, F., Parol, F., Riédi, J., and Vanbauce, C.: Toward New Inferences about Cloud Structures from Multidirectional Measurements in the Oxygen A Band: Middle-of-Cloud Pressure and Cloud Geometrical Thickness from POLDER-3/PARASOL, J. Appl. Meteorol. Climatol., 49, 2492–2507, 2010. 2537, 2540, 2541, 2543, 2544, 2545, 2548, 2550, 2551, 2555

Fischer, J. and Grassl, H.: Detection of Cloud-Top-Height from Backscattered Radiances within the Oxygen A Band. Part 1: Theoretical Study, J. Appl. Meteorol., 30, 1245–1259, 1991. 2536

Fischer, J., Cordes, W., Schmitz-Peiffer, A., Renger, W., and Mörl, P.: Detection of Cloud-Top-Height from Backscattered Radiances within the Oxygen A Band. Part 2: measurements, J. Appl. Meteorol., 30, 1260–1267, 1991. 2536

Fournier, N., Stammes, P., de Graaf, M., van der A, R., Piters, A., Grzegorski, M., and Kokhanovsky, A.: Improving cloud information over deserts from SCIAMACHY Oxygen A-band measurements, Atmos. Chem. Phys., 6, 163–172, doi:10.5194/acp-6-163-2006, 2006. 2537

Goloub, P., Deuze, J. L., Herman, M., and Fouquart, Y.: Analysis of the POLDER polarization measurements performed over cloud covers, IEEE Trans. Geosci. Remote Sens., 32, 78–88, 1994. 2536

Holz, R. E., Ackerman, S. A., Nagle, F. W., Frey, R., Dutcher, S., Kuehn, R. E., Vaughan, M. A., and Baum, B.: Global Moderate Resolution Imaging Spectroradiometer (MODIS) cloud detection and height evaluation using CALIOP, J. Geophys. Res., 113, D00A19, doi:10.1029/2008JD009837, 2008. 2547

Knibbe, W. J. J., de Haan, J. F., Hovenier, J. W., Stam, D. M., Koelemeijer, R. B. A., and Stammes, P.: Deriving terrestrial cloud top pressure from photopolarimetry of reflected light, J. Quant. Spectrosc. Ra., 64, 173–199, 2000. 2536

Koelemeijer, R. B. A., Stammes, P., Hovenier, J. W., and de Haan, J. F.: Global distributions of effective cloud fraction and cloud top pressure derived from oxygen A band spectra measured by the Global Ozone Monitoring Experiment: Comparison to ISCCP data, J. Geophys. Res., 107, AAC 5-1–AAC 5-9, doi:10.1029/2001JD000840, 2002. 2537

Kuze, A. and Chance, K. V.: Analysis of cloud top height and cloud coverage from satellites using the O_2 A and B bands, J. Geophys. Res., 99, 14481–14492, 1994. 2536

Li, S. and Min, Q.: Diagnosis of multilayer clouds using photon path length distributions, J. Geophys. Res., 115, D20202, doi:10.1029/2009JD013774, 2010. 2535

Lindstrot, R., Preusker, R., Ruhtz, T., Heese, B., Wiegner, M., Lindemann, C., and Fischer, J.: Validation of MERIS cloud top pressure using airborne lidar measurements, J. Appl. Meteorol. Climatol, 45, 1612–1621, 2006. 2537

Mace, G. G., Zhang, Q., Vaughan, M., Marchand, R., Stephens, G., Trepte, C., and Winker, D.: A description of hydrometeor layer occurrence statistics derived from the first year of merged Cloudsat and CALIPSO data, J. Geophys. Res., 114, D00A26, doi:10.1029/2007JD009755, 2009. 2535

Menzel, W. P., Frey, R. A., Zhang, H., Wylie, D. P., Moeller, C. C., Holz, R. E., Maddux, B., Baum, B. A., Strabala, K. I., and Gumley, L. E.: MODIS Global Cloud-Top Pressure and Amount Estimation: Algorithm Description and Results, J. Appl. Meteorol. Climatol., 47, 1175–1198, 2008. 2536

Parol, F., Buriez, J.-C., Vanbauce, C., Couvert, P., Séze, G., Goloub, P., and Cheinet, S.: First results of the POLDER "Earth Radiation Budget and Clouds" operational algorithm, IEEE Trans. Geosci. Remote Sens., 37, 1597–1612, 1999. 2540

Press, W. H., Teukolsky, S. A., Vetterling, W. T., and Flannery., B. P.: numerical Recipes in Fortran 77: The Art of Scientific Computing, 2nd Edn., Cambridge university Press, 1992. 2549

Preusker, R. and Lindstrot, R.: Remote Sensing of Cloud-Top Pressure Using Moderately Resolved Measurements within the Oxygen A Band – A Sensitivity Study, J. Appl. Meteorol. Climatol., 48, 1562–1574, 2009. 2537

Preusker, R., Fischer, J., P., A., Bennartz, R., and Schüller, L.: Cloud-top pressure retrieval using the oxygen A-band in the IRS-3 MOS intrument, Int. J. Remote. Sens., 28, 1957–1967, 2007. 2537

Rienecker, M.: File specification for GEOS-5 DAS gridded output. Global Modeling and Assimilation Office Doc. GMAO-1001v6.4, Tech. Rep., 54 pp., 2008. 2542

Rossow, W. B. and Schiffer, R. A.: Advances in understanding clouds from ISCCP, Bull. Am. Meteor. Soc., 80, 2261–2287, 1999. 2535, 2544

Rothman, L. S., Jacquemarta, D., Barbeb, A., Chris Bennerc, D., Birkd, M., Browne, L. R., Carleerf, M. R., Chackerian Jr., C., Chancea, K., Couderth, L. H., Danai, V., Devic, V. M., Flaudh, J.-M., Gamachej, R. R., Goldmank, A., Hartmannh, J.-M., Jucksl, K. W., Makim, A. G., Mandini, J.-Y., Massien, S. T., Orphalh, J., Perrinh, A., Rinslando, C. P., Smitho, M. A. H., Tennysonp, J., Tolchenovp, R. N., Tothe, R. A., Vander Auweraf, J., Varanasiq, P., and Wagnerd, G.: The HITRAN molecular spectroscopic database, J. Quant. Spectrosc. Ra., 96, 139–204, 2005. 2539

Saiedy, F., Hilleary, D. T., and Morgan, W. A.: Cloud-top altitude measurements from satellites, Appl. Opt., 4, 495–500, 1965. 2537

Scott, N.: A direct method of computation of transmission function of an inhomogeneous gaseous medium: description of the method and influence of various factors, J. Quant. Spectrosc. Ra., 14, 691, 1974. 2539

Seiz, G., Tjemkes, S., and Watts, P.: Multiview cloud-top height and wind retrieval with photogrammetric methods: Application to Meteosat-8 HRV observations, J. Appl. Meteorol. Climatol., 46, 1182–1195, 2007. 2536

Sneep, M., de Haan, J. F., Stammes, P., Wang, P., Vanbauce, C., Vasilkov, A. P., and Levelt, P. F.: Three-way comparison between OMI and PARASOL cloud pressure products, J. Geophys. Res., 113, D15S23, doi:10.1029/2007JD008694, 2008. 2537, 2540

Stephens, G. L.: Radiation profiles in extended water clouds. I: Theory, J. Atmos. Sci., 35, 2111–2122, 1978. 2535

Stephens, G. L., Vane, D. G., Boain, R. J., Mace, G. G., Sassen, K., Wang, Z., Illingworth, A. J., O'Connor, E. J., Rossow, W. B., Durden, S. L., Miller, S. D., Austin, R. T., Benedetti, A., Mitrescu, C., and The CloudSat Science Team: The CloudSat mission and the A Train, A New Dimension of Space-Based Observations of Clouds and Precipitation, Bull. Am. Meteorol. Soc., 83, 1771–1790, 2002. 2538

AMTD
6, 2533–2581, 2013

Improved information about clouds from POLDER3

M. Desmons et al.

Stubenrauch, C. J., Chédin, A., Rädel, G., Scott, N. A., and Serrar, S.: Cloud Properties and Their Seasonal and Diurnal Variability from TOVS Path-B, J. Climate, 19, 5531–5553, 2006. 2543, 2550

van de Hulst, H. C.: Multiple Light Scattering. Tables, Formulas and Applications, Volume 2, Academic Press, 1980. 2537, 2541

Vanbauce, C., Buriez, J., Parol, F., Bonnel, B., Seze, G., and Couvert, P.: Apparent pressure derived from ADEOS-POLDER observations in the oxygen A-band over ocean, Geophys. Res. Lett., 25, 3159–3162, 1998. 2537, 2540

Vanbauce, C., Cadet, B., and Marchand, R.: Comparison of POLDER apparent and corrected oxygen pressure to ARM/MMCR cloud boundary pressures, Geophys. Res. Lett., 30, 16.1–16.4, 2003. 2537, 2540

Wang, J., Rossow, W., and Zhang, Y.: Cloud Vertical Structure and Its Variations from a 20-Yr Global Rawinsonde Dataset, J. Climate, 13, 3041–3056, 2000. 2543

Wang, P., Stammes, P., van der A, R., Pinardi, G., and van Roozendael, M.: FRESCO+: an improved O_2 A-band cloud retrieval algorithm for tropospheric trace gas retrievals, Atmos. Chem. Phys., 8, 6565–6576, doi:10.5194/acp-8-6565-2008, 2008. 2537, 2540

Warren, S. G., Eastman, R., and Hahn, C. J.: Cloud Climatology. Encyclopedia of Atmospheric Sciences, 2nd Edn., Oxford University Press, 2012. 2543

Weisz, E., Li, J., Zhou, D. K., Huang, H.-L., Goldberg, M. D., and Yang, P.: Cloudy sounding and cloud-top height retrieval from AIRS alone single field-of-view radiance measurements, Geophys. Res. Lett., 34, L12802, doi:10.1029/2007GL030219, 2007. 2536

Wielicki, B. A. and Coakley, J. A.: Cloud retrieval using infrared sounder data: Error analysis, J. Appl. Meteorol., 20, 157–169, 1981. 2536

Winker, D. M. and Trepte, C. R.: Laminar cirrus observed near the tropical tropopause by LITE, Geophys. Res. Lett., 25, 3351–3354, 1998. 2535

Winker, D. M., Hunt, W. H., and McGill, M. J.: Initial performance assessment of CALIOP, Geophys. Res. Lett., 34, L19803, doi:10.1029/2007GL030135, 2007. 2535

Wu, D. L., Ackerman, S. A., Davies, R., Diner, D. J., Garay, M. J., Kahn, B. H., Maddux, B. C., Moroney, C. M., Stephens, G. L., Veefkind, J. P., and Vaughan, M. A.: Vertical distributions and relationships of cloud occurrence frequency as observed by MISR, AIRS, MODIS, OMI, CALIPSO, and CloudSat, Geophys. Res. Lett., 36, L09821, doi:10.1029/2009GL037464, 2009. 2536

AMTD
6, 2533–2581, 2013

Improved information about clouds from POLDER3

M. Desmons et al.

Wu, M. L.: Remote Sensing of cloud-top pressure using reflected solar radiation in the oxygen A-band, J. Appl. Meteorol., 24, 539–546, 1985. 2536

Yamamoto, G. and Wark, D. Q.: Discussion of the letter by R. A. Hanel, “Determination of cloud altitude from a satellite”, J. Geophys. Res., 66, 3596–3596, doi:10.1029/JZ066i010p03596, 1961. 2537

Yang, Y., Marshak, A., Mao, J., Lyapustin, A., and Herman, J.: A method of retrieving cloud top height and cloud geometrical thickness with oxygen A and B bands for the Deep Space Climate Observatory (DSCOVR) mission: Radiative transfer simulations, J. Quant. Spectrosc. Ra., doi:10.1016/j.jqsrt.2012.09.017, in press, 2012. 2537

Table 1. Level 2 A-Train data (daytime only) used in our study at 5 km horizontal sampling.

Product	Dataset	Horizontal resolution	Sensor (satellite)
RB2_ v16	Cloud oxygen pressure P_{O_2} Cloud oxygen pressure angular standard deviation $\sigma_{P_{O_2}}$ Cloud cover "cc" Cloud phase Cloud optical thickness τ Cosine of the solar zenith angle μ_s Surface type index	$18 \times 21\,km^2$	POLDER3 (PARASOL)
2B-GEOPROF-LIDAR.V04	Number of cloud layers n Cloud top altitudes LAYERTOP Cloud base altitudes LAYER-BASE	5 km	CPR/CALIOP (CloudSat/CALIPSO)
MYD06_L2.C5	Cloud top pressure: MODIS CTP	5 km	MODIS (Aqua)
	Cloud phase	5 km	

AMTD
6, 2533–2581, 2013
Improved information about clouds from POLDER3
M. Desmons et al.

Table 2. Statistics of the inversion of H for liquid water clouds and ice clouds in 2008 over ocean and land. Values are in meters.

	Liquid water clouds					
	Ocean			Land		
Method	ΔH	SD	MD	ΔH	SD	MD
$\sigma_{P_{O_2}}$	5	964	180	23	1146	300
ΔP	−12	1193	−21	−272	1425	−202
Mean	−17	983	73	−138	1186	61
	Ice clouds					
	Ocean			Land		
Method	ΔH	SD	MD	ΔH	SD	MD
ΔP	1580	5803	−26	857	4859	−227

AMTD
6, 2533–2581, 2013

Improved information about clouds from POLDER3

M. Desmons et al.

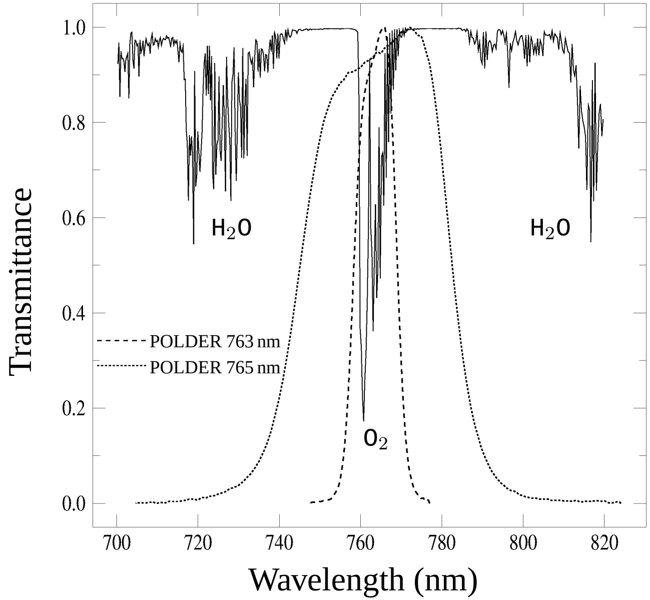

Fig. 1. Atmospheric transmission in the oxygen A band region at the resolution of $5\,cm^{-1}$ ($\simeq 0.3$ nm) (for an air mass equal to 1 and a standard midlatitude summer atmosphere). The filter's transmissions of the two POLDER O_2 bands (centered at 763 and 765 nm with a 10 nm and 40 nm FWHM) are also given in dashed lines.

AMTD
6, 2533–2581, 2013

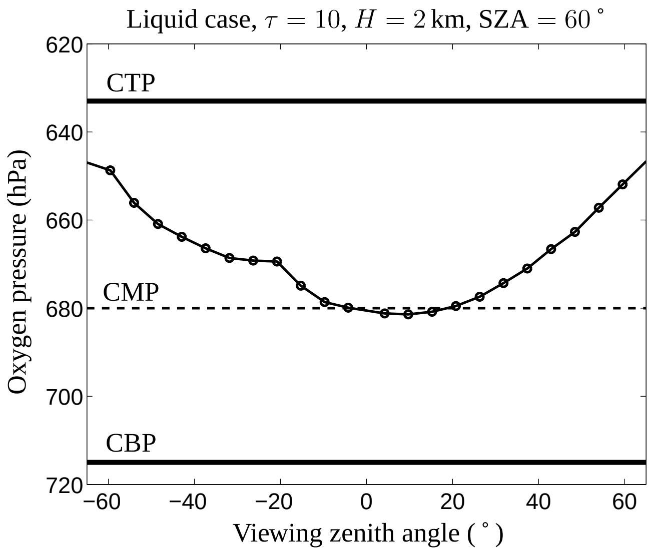

Fig. 2. Variation of simulated POLDER cloud oxygen pressure P_{O_2} with the viewing zenith angles of upwelling directions for a particular case study – Horizontal lines indicate the level of cloud top, middle, and base pressures (noted respectively CTP, CMP and CBP). The angularly averaged oxygen pressure is here 667 hPa and the angular standard deviation 11 hPa – Discontinuities of P_{O_2} signal at −60° and −20° are signatures of cloud scattering phase function.

AMTD
6, 2533–2581, 2013

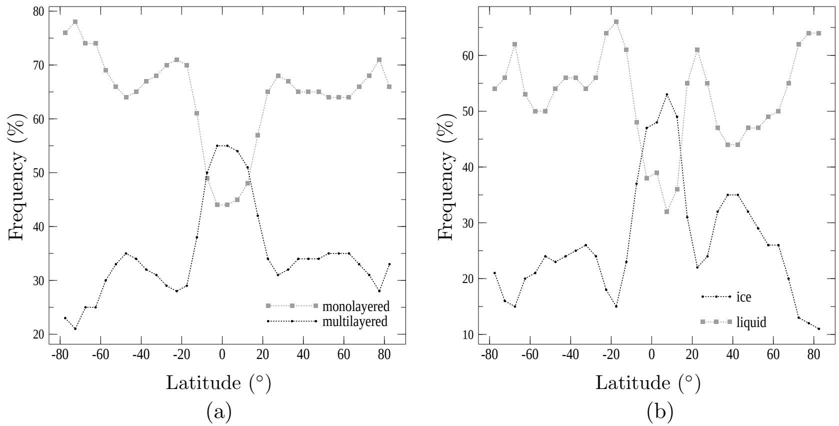

Fig. 3. Climatology of clouds in 2008: panel **(a)** provides the occurences (in %) of monolayered (grey line) and multilayered (black line) clouds; panel **(b)** provides the occurences (in %) of liquid water (grey line) and ice (black line) clouds among monolayered clouds.

AMTD
6, 2533–2581, 2013

Title Page
Abstract | Introduction
Conclusions | References
Tables | Figures
◀| |▶
◀ ▶
Back | Close
Full Screen / Esc
Printer-friendly Version
Interactive Discussion

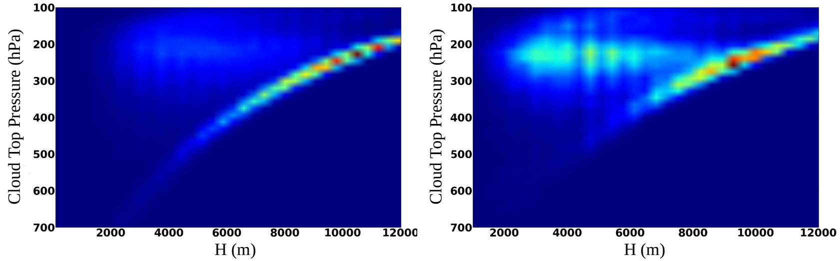

(a) Monolayer ice clouds (over ocean and land (left and right panel respectively))

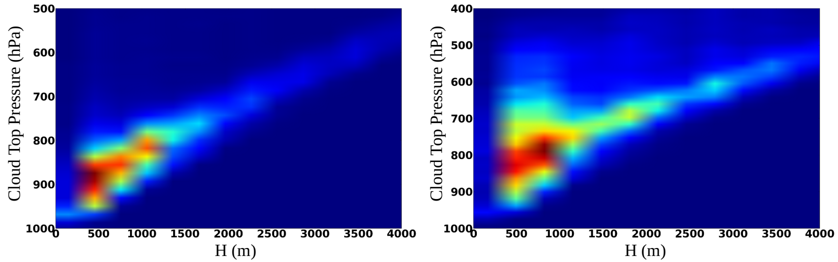

(b) Monolayer liquid clouds (over ocean and land (left and right panel respectively))

Fig. 4. Climatology of monolayer clouds in 2008: CALIOP/CloudSat Cloud Top Pressure – Vertical extension occurences, over ocean on the left panels, over land on the right panels.

AMTD
6, 2533–2581, 2013

Title Page
Abstract | Introduction
Conclusions | References
Tables | Figures
◀| |▶
◀ ▶
Back | Close
Full Screen / Esc
Printer-friendly Version
Interactive Discussion

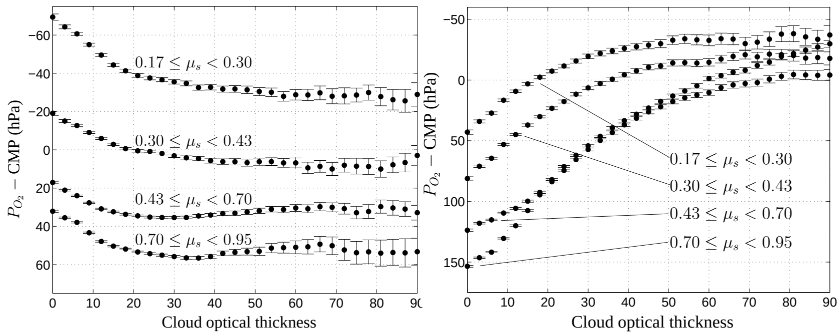

(a) For liquid water clouds

(b) For ice water clouds

Fig. 5. Difference between POLDER oxygen pressure and actual cloud middle pressure (CMP) from CloudSat/CALIPSO as a function of cloud optical thickness, on average in 2008 and by classes of solar zenith angle's cosine. Standard deviation are indicated.

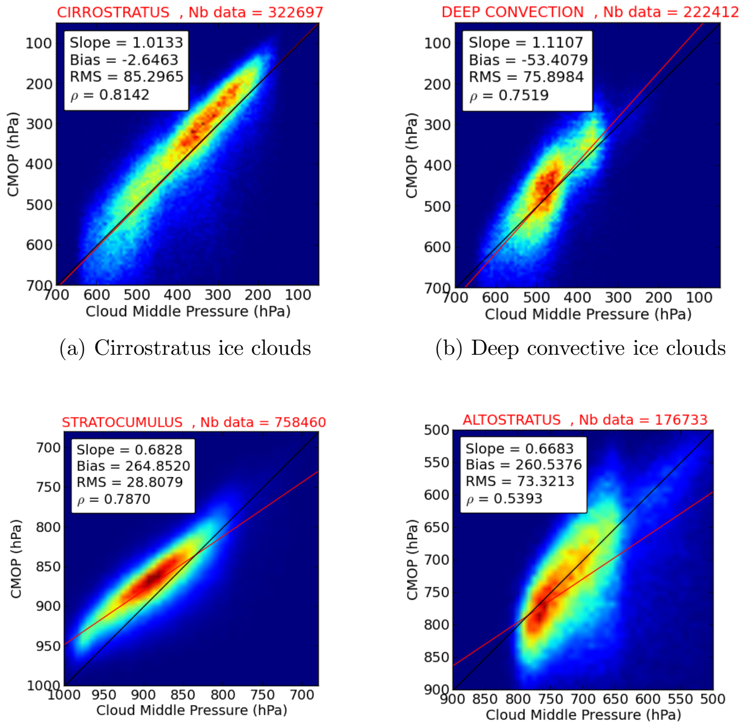

(a) Cirrostratus ice clouds

(b) Deep convective ice clouds

(c) Stratocumulus liquid water clouds

(d) Altostratus liquid water clouds

Fig. 6. Comparison between POLDER cloud middle oxygen pressure (CMOP) and CloudSat/CALIPSO cloud middle pressure CMP. Cases of clouds over ocean in 2008.

AMTD
6, 2533–2581, 2013

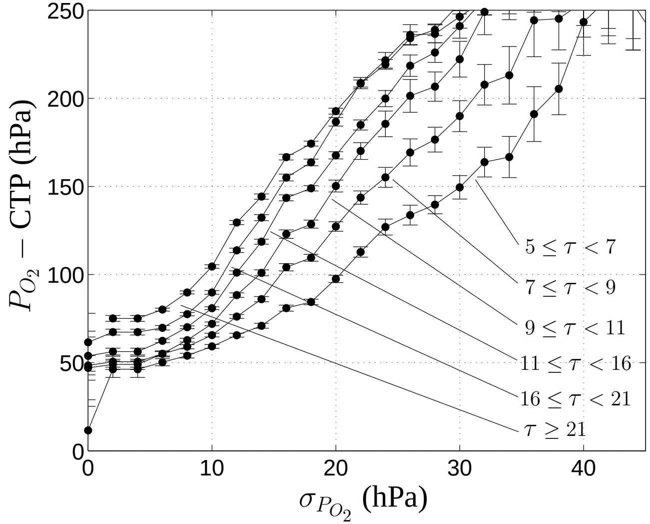

Fig. 7. Relation between P_{O_2} – CTP and $\sigma_{P_{O_2}}$ on average in 2008. Case of liquid water clouds over ocean, and for particular solar conditions: $0.7 \leq \mu_s \leq 0.8$. Standard deviation are also shown.

AMTD
6, 2533–2581, 2013

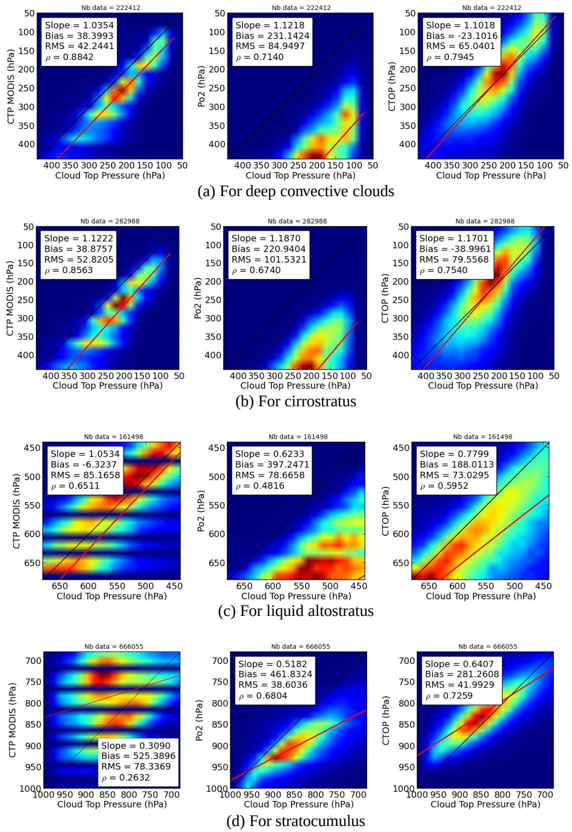

Fig. 8. Comparison above ocean in 2008 between cloud top pressure (from CloudSat/CALIPSO) and POLDER pressures (historical pressure P_{O_2} and new cloud top oxygen pressure (CTOP) in the middle and right panels respectively). The left side panels show for comparison MODIS cloud top pressures.

Discussion Paper | Discussion Paper | Discussion Paper | Discussion Paper |

AMTD

6, 2533–2581, 2013

Improved information about clouds from POLDER3

M. Desmons et al.

Title Page
Abstract Introduction
Conclusions References
Tables Figures
Back Close
Full Screen / Esc
Printer-friendly Version
Interactive Discussion

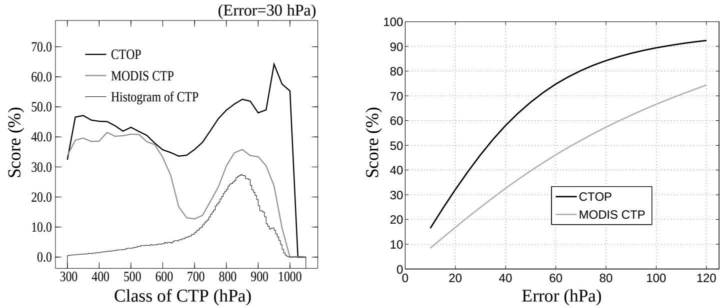

(a) Case of liquid water clouds

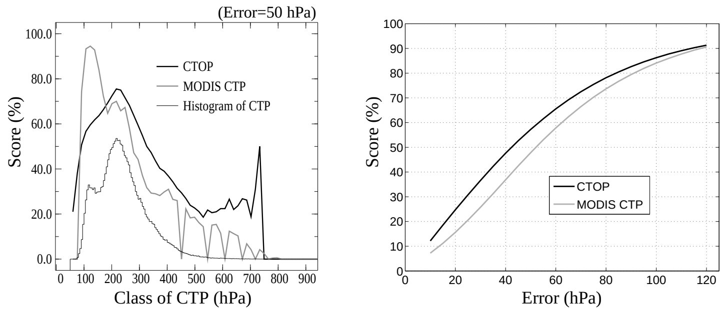

(b) Case of ice clouds

Fig. 9. Scores obtained over ocean by the cloud top pressure estimates CTOP and MODIS CTP for liquid water clouds (case a) and ice clouds (case b). Scores in left panels are given per class of CTP, and correspond to an error of 30 and 50 hPa for liquid and ice clouds respectively. Right panels show global scores as a function of pressure errors. Thick black lines are for CTOP, thick grey for MODIS CTP. Histograms of CTP are also plotted in left panels (thin black lines, in arbitrary units).

AMTD
6, 2533–2581, 2013

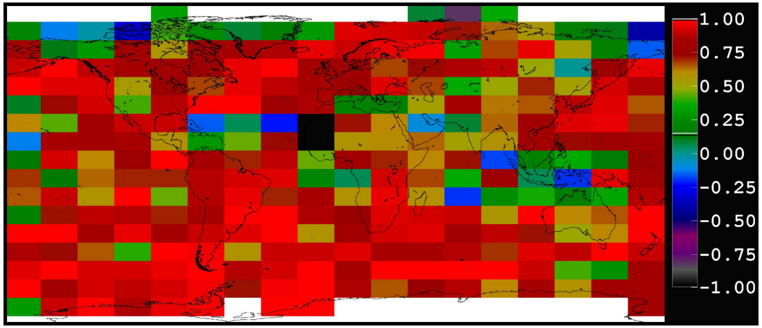

Fig. 10. Correlation coefficient between $\sigma_{P_{O_2}}$ and H by areas of 10° of latitude and 20° of longitude. Cases of monolayered liquid clouds in 2008.

AMTD
6, 2533–2581, 2013

Improved information about clouds from POLDER3

M. Desmons et al.

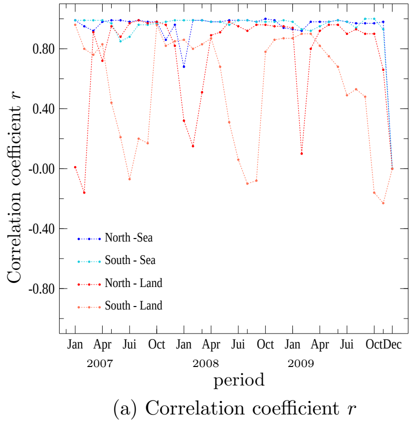

(a) Correlation coefficient r

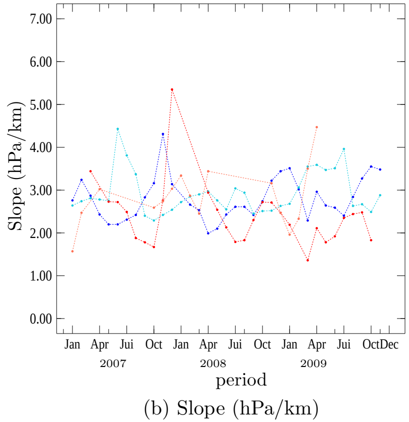

(b) Slope (hPa/km)

Fig. 11. Temporal evolution of the correlation between $\sigma_{P_{O_2}}$ and H month by month from 2007 to 2009. Cases of monolayered liquid clouds with $\tau \geq 5$ and $cc \geq 0.95$.

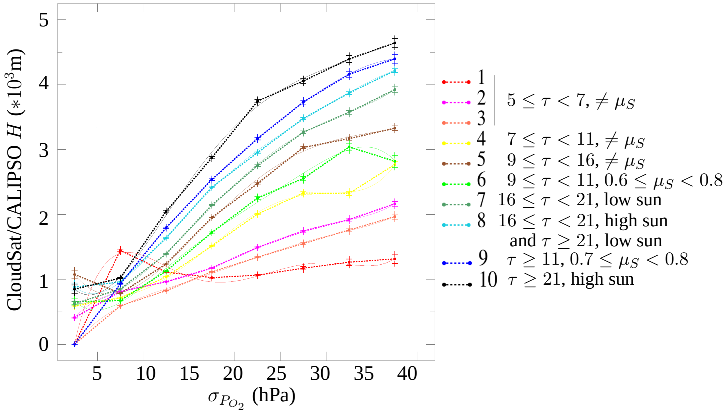

Fig. 12. Average relation (H, $\sigma_{P_{O_2}}$) and 5-order fits for classes of τ and μ_s. Cases of monolayered liquid clouds in 2008 over ocean, with $\tau \ge 5$ and $cc \ge 0.95$

Discussion Paper | Discussion Paper | Discussion Paper | Discussion Paper |

AMTD

6, 2533–2581, 2013

Improved information about clouds from POLDER3

M. Desmons et al.

AMTD
6, 2533–2581, 2013

Improved information about clouds from POLDER3

M. Desmons et al.

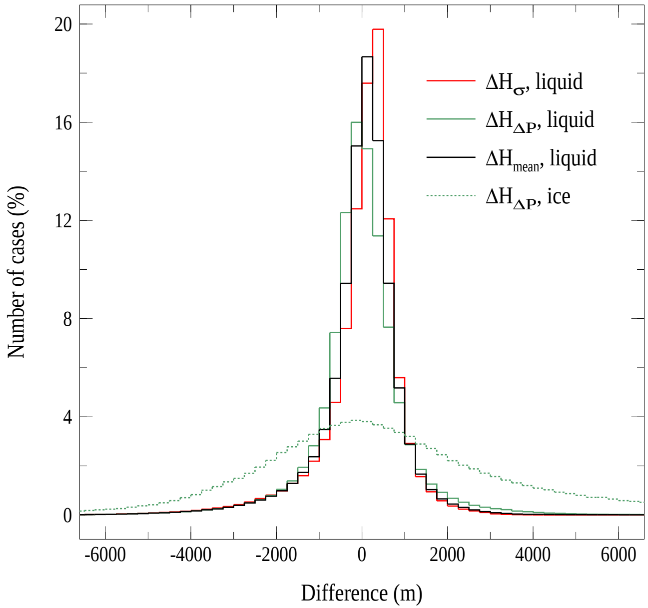

Fig. 13. Histogram of the difference between the CloudSat/CALIOP H and the retrieved H for liquid water clouds (solid line) and ice clouds (dashed line) over ocean in 2008. On the red curve, H was retrieved from $\sigma_{P_{O_2}}$, on the green one, it was retrieved from ΔP. For liquid water clouds , the black curve shows the difference between H_{mean} and H (see text for explanation).

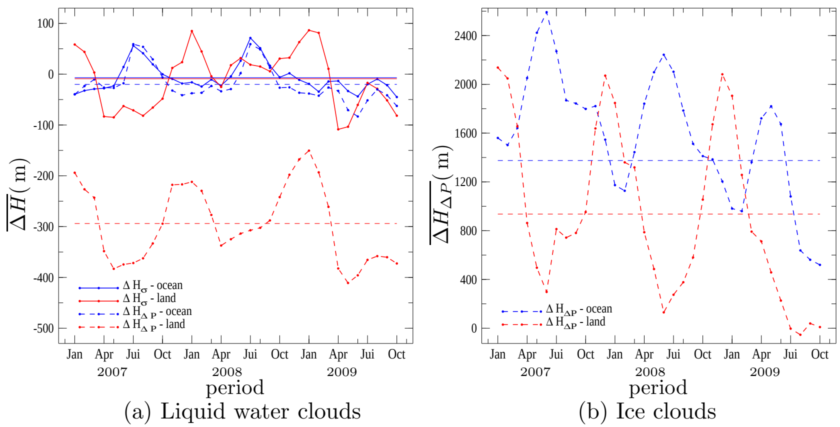

Fig. 14. Temporal evolution of the monthly average difference between CloudSat/CALIOP H and the retrieved H from 2007 to 2009 for liquid water clouds (panel **(a)**, $H_{\Delta P}$ and $H_{\Delta P}$ in solid and dashed line respectively) and ice clouds (panel **(b)**, $H_{\Delta P}$ in dashed line). In blue over ocean, and red over land. The standard deviation is not represented as it stays close to 1000 m (resp. 5000 m) for liquid (resp. ice) clouds all along the three years.

AMTD
6, 2533–2581, 2013

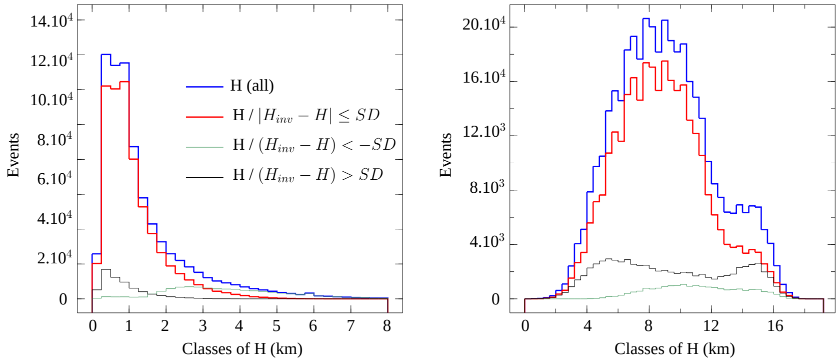

(a) Liquid water clouds

(b) Ice clouds

Fig. 15. Histograms of cloud geometrical thickness for monolayer liquid **(a)** and ice **(b)** clouds in 2008 over ocean: all clouds (blue line), clouds for which the retrieval of H is less biased (red line), clouds for which the retrieval underestimates H (thin dark green line) or overestimates it (thin black line). SD stands for Standard Deviation.

AMTD

6, 2533–2581, 2013

Improved information about clouds from POLDER3

M. Desmons et al.

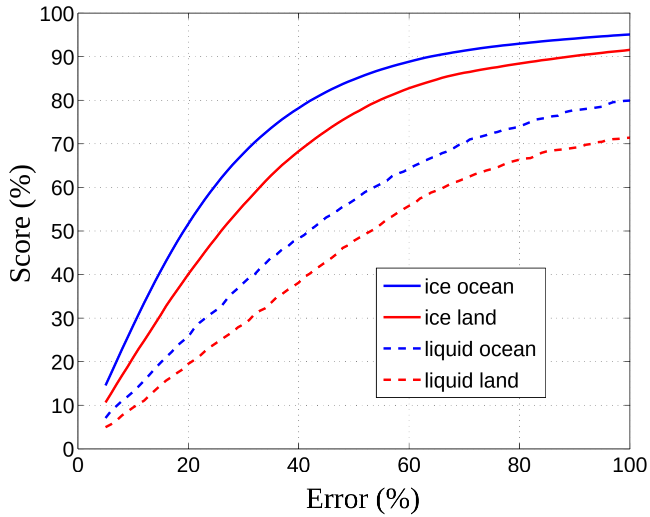

Fig. 16. Scores obtained by the estimates of cloud vertical extent *H* for liquid water and ice clouds as a function of retrieval errors in percent.

AMTD
6, 2533–2581, 2013

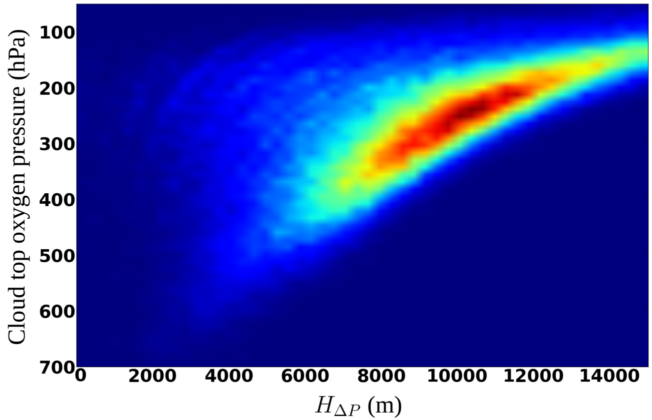

Fig. 17. POLDER based climatology of monolayer ice clouds over ocean in 2008: Cloud top oxygen pressure (CTOP) vs cloud vertical extension $H_{\Delta P}$ occurences. To be compared with the top left panel of Fig. 4

AMTD
6, 2533–2581, 2013

Improved information about clouds from POLDER3

M. Desmons et al.